NUMERICAL INVESTIGATION ON THE PERFORMANCE OF SUPERSONIC EJECTOR USING CFD

Thaís Piva de Castro, tha.piva@gmail.com
Edson Luiz Zaparoli, zaparoli@ita.br
Cláudia Regina de Andrade, claudia@ita.br
Instituto Tecnológico de Aeronáutica, Departamento de Engenharia Aeronáutica e Mecânica, Área de Aerodinâmica, Propulsão e Energia – Praça Marechal Eduardo Gomes, 50, Vila das Acácias, CEP 12.228-900, São José dos Campos, SP, Brasil.

Abstract. *Supersonic ejectors are widely used in different applications such as aerospace, propulsion and refrigeration. The ejector is characterised by the use of the kinetic energy of one fluid stream (the primary fluid) to drive a second fluid stream (the secondary fluid) by direct mixing. An ejector is a simple device since that it consists of four main unmoving components: primary nozzle, secondary inlet, mixing chamber and diffuser. This type of device is attractive due the lack of moving parts, low cost and high reliability. The performance of a gas driven supersonic ejector depends upon its geometry (shape, layout and dimensions), the properties of the gas and secondary fluid (density, molecular weight and specific heat ratios), the flow conditions (pressures, temperatures, mass flow rates) at the primary and secondary inlets and the diffuser outlet. Although the gas driven ejector is conceptually a simple device, the physical processes that occur in flow are extremely complex. In this work the mathematical model of this compressible flow is numerically solved using finite volume method with a coupled pressure-based approach. An adaptive mesh refinement is employed to capture shock reflections and shock-mixing layer interaction. Numerical results for the ejector efficiency was compared with available experimental literature data. Finally, it was done a numerical simulation varying the constant pressure mixing chamber length and mass flow at secondary inlet.*

Keywords*: CFD, ejector, supersonic*

1. INTRODUCTION

The ejector was invented by Sir Charles Parsons around 1901, and in 1910 an ejector was used by Maurice Leblanc in the first steam jet refrigeration system. An ejector is a simple device since that it consists of four main unmoving components: primary nozzle, secondary inlet, mixing chamber and diffuser, Fig .1, and is widely used in different applications such as aerospace, propulsion and refrigeration. This type device is attractive due to lack of moving parts, low cost and high reliability.

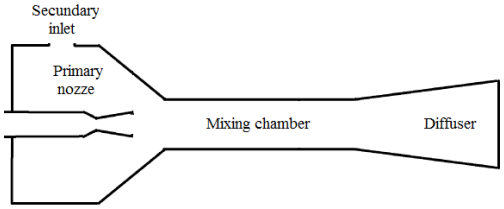

Figure 1. Ejector configuration

Bartosiewicz et al. (2005) performed numerical and experimental investigations to obtain a reliable hydrodynamics model of a supersonic ejector for refrigeration application. In the first part of their work, the performance of six turbulence models is evaluated in terms of correct representation of physical phenomena for supersonic ejectors, in the second part, the tested model was used to simulate the different operation modes of a supersonic ejector, ranging from on-design point to off-design. The work showed that the RNG and sst - k – ω models were the best suited to predict the shock, strength, and the mean line pressure recovery. However, the sst - k – ω model has shown better performances in term of stream mixing. In another study Bartosiewicz et al. (2006) used the CFD modeling to study the flow structure and operation under various operating conditions. This was the first paper dealing with local CFD modeling that takes into account shock–boundary layer interactions in a real refrigerant. The numerical results obtained, contribute to understanding the local structure of the flow and demonstrate the crucial role of the secondary nozzle for the mixing rate performance. They concluded that entrainment performance is mainly built in the secondary nozzle, while recompression is achieved in the mixing chamber. They concluded also that the strong shocks waves occurring at the secondary nozzle exit can dramatically decrease the mixing rate and even reverse the flow and the CFD software can predict ejector malfunction.

Sriveerakul et al. (2007a) presented a CFD analysis in order to predict the performance of a steam ejector used in refrigeration applications. This study was reported in two papers. The first, Sriveerakul et al. (2007a), presented an investigation on the effects of operating conditions and geometries on steam ejector and, in the second, Sriveerakul et al. (2007b), concentrated on the use of CFD in visualizing the change in the flow structure and the mixing process inside the steam ejector as influenced by interested parameters, ejector's operating conditions and geometries. The CFD visualization shows two series of oblique shocks. The first series was found immediately after the primary fluid stream leaves the primary nozzle and begins to mix with the secondary fluid stream. The second series of oblique shock was found at the beginning of the diffuser section as a result of a non-uniform mixed stream. It can be seen that both entrainment ratio and critical back pressure can be varied simultaneously by adjusting three parameters, the primary fluid saturated pressure, the secondary fluid saturated pressure, and the primary nozzle size.

Yinhai et al. (2009) presented a Computational Fluid Dynamics (CFD) analysis the effects of two important ejector geometry parameters: the primary nozzle exit position (NXP) and the mixing section converging angle h, on its performance. The author created 95 different ejector geometries and tested under different working conditions. From 210 testing results, it is found that the optimum NXP is not only proportional to the mixing section throat diameter, but also increases as the primary flow pressure rises. On the other hand, the ejector performance is very sensitive to h, especially near to the optimum working point. A relatively bigger h is required to better maximize the ejector performance when the primary flow pressure rises.

This work presents a numerical study about supersonic gas ejector based on geometric parameters provided by Bartosiewicz et al. (2005) and Desevaux (2001). The mathematical model is numerically solved (continuity, momentum, energy and realizable $k-\varepsilon$ or sst$-k-\omega$ turbulence model) using finite volume method in order to investigate the ejector performance, analyzing the influence of the turbulence models, the geometry the constant pressure mixing chamber length and mass flow at secondary inlet.

2. PROBLEM DEFINITION

In the ejector, "Fig. 2", the primary fluid a high pressure and temperature expands and accelerates through the primary nozzle convergent-divergent (i), reaches sonic velocity in the throat and is ejected with supersonic velocity to create a very low pressure region at the primary nozzle exit (ii) and subsequently in the mixing chamber. This means "a secondary fluid" can be entrained into the mixing chamber. The speed of the secondary fluid rises to sonic value (iii) and chokes. Then the mixing process begins. This mixing causes the primary flow to be retarded whilst secondary flow is accelerated. By the end of the mixing chamber, the two streams are completely (iv). Due to a high pressure region downstream of the mixing chamber's throat, a normal shock of essentially zero thickness is induced (v). This shock causes a major compression effect and a sudden drop in the flow speed from supersonic to subsonic. A further compression of the flow is achieved (vi) as it is brought to stagnation through a subsonic diffuser.

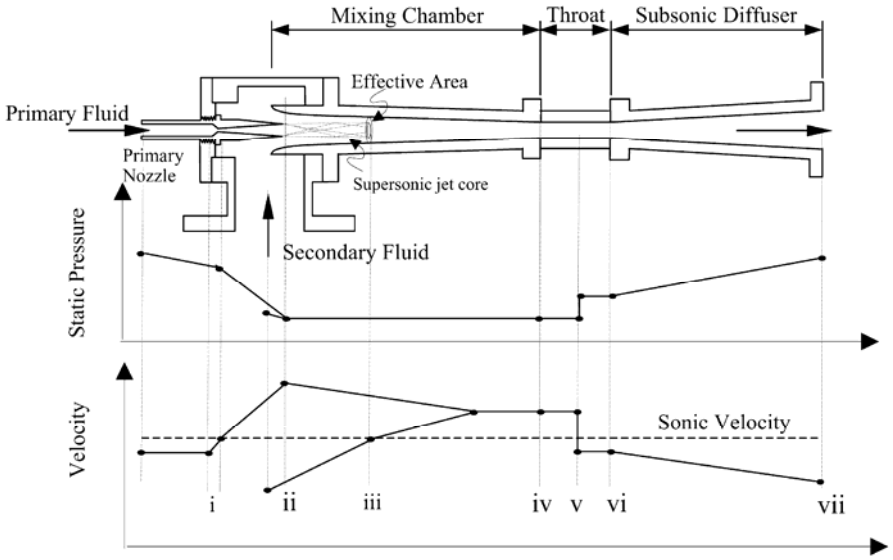

Figure 2. Schematic view and the variation of stream pressure and velocity as a function of location along an ejector, Sriveerakul et al. (2007a).

3. MATHEMATICAL MODELING

The mathematical formulation can be described, in cartesian form, by continuity, momentum, energy and turbulence models equations (realizable – k– ε or sst – k– ω), Eqs. (1) to (9), respectively. Following assumptions were taken into account: two dimensional, axisymmetrical, compressible, ideal gas, air flow, unsteady state regime and constants transport properties.

Continuity equation

$$\frac{\partial \rho}{\partial t}+\frac{\partial}{\partial x_i}(\rho u_i)=0 \tag{1}$$

Momentum equation

$$\frac{\partial}{\partial t}(\rho u_i)+\frac{\partial}{\partial x_j}(\rho u_i u_j)=-\frac{\partial P}{\partial x_i}+\frac{\partial \tau_{ij}}{\partial x_j} \tag{2}$$

where stress tensor components are evaluated as:

$$\tau_{ij}=\left(\mu+\mu_t\right)\left(\frac{\partial u_j}{\partial x_i}+\frac{\partial u_i}{\partial x_j}\right)-\frac{2}{3}\left(\mu+\mu_t\right)\frac{\partial u_k}{\partial x_k}\delta_{ij}$$

Energy equation

$$\frac{\partial}{\partial t}(\rho E)+\frac{\partial}{\partial x_j}(u_j(\rho E+P))=\frac{\partial}{\partial x_j}\left[\Gamma_E\frac{\partial T}{\partial x_j}+u_i\left(\tau_{ij}\right)\right] \tag{3}$$

Equations of the realizable – k– ε model

$$\frac{\partial}{\partial t}(\rho k)+\frac{\partial}{\partial x_j}(\rho k u_j)=\frac{\partial}{\partial x_j}\left[\left(\mu+\frac{\mu_t}{\sigma_k}\right)\frac{\partial k}{\partial x_j}\right]+G_k-\rho\varepsilon-Y_M \tag{4}$$

$$\frac{\partial}{\partial t}(\rho \varepsilon)+\frac{\partial}{\partial x_j}(\rho \varepsilon u_j)=\frac{\partial}{\partial x_j}\left[\left(\mu+\frac{\mu_t}{\sigma_\varepsilon}\right)\frac{\partial \varepsilon}{\partial x_j}\right]-\rho C_2\frac{\varepsilon^2}{k+\sqrt{v\varepsilon}} \tag{5}$$

The constant values of the realizable k– ε model used in this work are: $\sigma_k=1.0$; $\sigma_\varepsilon=1.2$; $C_2=1.9$

The eddy viscosity is computed from:

$$\mu_t=\rho C_\mu\frac{k^2}{\varepsilon} \tag{6}$$

where

$$C_\mu=\frac{1}{A_0+A_S\dfrac{KU^*}{\varepsilon}}\ ;\ U^*\equiv\tilde{S}=\sqrt{S_{ij}S_{ij}}\ ;\ A_0=4.04\ ;\ A_S=\sqrt{6}\cos\phi\ ;\ \phi=\frac{1}{3}\cos^{-1}\left(\sqrt{6}W\right);\ W=\frac{S_{ij}S_{jk}S_{ki}}{\tilde{S}^3}$$

Equations of the sst - k– ω model

$$\frac{\partial}{\partial t}(\rho k)+\frac{\partial}{\partial x_i}(\rho k u_i)=\frac{\partial}{\partial x_j}\left[\left(\mu+\frac{\mu_t}{\sigma_k}\right)\frac{\partial k}{\partial x_j}\right]+\tilde{G}_k-Y_k \tag{7}$$

$$\frac{\partial}{\partial t}(\rho\omega)+\frac{\partial}{\partial x_i}(\rho\omega u_i)=\frac{\partial}{\partial x_j}\left[\left(\mu+\frac{\mu_t}{\sigma_\omega}\right)\frac{\partial\omega}{\partial x_j}\right]+G_\omega-Y_\omega \tag{8}$$

The constant values of the sst - k– ω model used in this work are: $\sigma_{k,1}=1.176$; $\sigma_{k,2}=1.0$; $\sigma_{\omega,1}=2.0$; $\sigma_{\omega,2}=1.168$; $\alpha_\infty^*=1$; $R_k=6$; $\beta_i=0{,}072$;

The turbulent viscosity is computed from:

$$\mu_t=\frac{\rho k}{\omega}\frac{1}{\max\left[\frac{1}{\alpha^*},\frac{SF_2}{a_1\omega}\right]} \tag{9}$$

where

$$\sigma_k=\frac{1}{F_1/\sigma_{k,1}+(1-F_1)/\sigma_{k,2}};\ \sigma_\omega=\frac{1}{F_1/\sigma_{\omega,1}+(1-F_1)/\sigma_{\omega,2}};$$

$$\alpha^*=\alpha_\infty^*\left(\frac{\alpha_0^*+R_{e_t}/R_k}{1+R_{e_t}/R_k}\right);\ R_{e_t}=\frac{\rho k}{\mu\omega};\ \alpha_0^*=\frac{\beta_i}{3};$$

$$F_1=\tanh\left(\phi_1^4\right);\ F_2=\tanh\left(\phi_2^2\right)$$

$$\phi_1=\min\left[\max\left(\frac{\sqrt{k}}{0.09\omega y'},\frac{500\mu}{\rho y^2\omega}\right),\frac{4\rho k}{\sigma_{\omega,2}D_\omega^+ y^2}\right];\ \phi_2=\max\left(\frac{\sqrt{k}}{0.09\omega y'},\frac{500\mu}{\rho y^2\omega}\right)$$

$$D_\omega^+=\max\left[2\rho\frac{1}{\sigma_{\omega,2}}\frac{1}{\omega}\frac{\partial k}{\partial x_j}\frac{\partial\omega}{\partial x_j},10^{-10}\right];$$

Table 1. Symbols.

C_2;	constant of the k - ε model
G_k and $\tilde{G}k$;	generation of turbulence kinetic energy due to the mean velocity gradients
G_ω;	represents the generation of ω
P;	Pressure
S_{ij};	Mean strain rate $S_{ij}=\frac{1}{2}\left(\frac{\partial u_j}{\partial x_i}-\frac{\partial u_i}{\partial x_j}\right)$
T;	Temperature
U^*;	mean velocity
Y_M;	the contribution of the fluctuating dilatation in compressible turbulence to the overall dissipation rate
Y_k and Y_ω;	dissipation of k and ω due to turbulence
k;	turbulence kinetic energy
v;	kinematic viscosity
ε;	dissipation rate
μ;	molecular dynamic fluid viscosity
ρ;	fluid density

μ_t ;	turbulent dynamic fluid viscosity
ω :	specific dissipation rate
σ_k , σ_ε and σ_ω ;	turbulent Prandtl numbers for (k), (ε) and (ω), respectively
$\Gamma_E = \Gamma + \Gamma_T$;	effective thermal conductivity
i, j, k ;	space components

Boundary conditions

In this work, the geometrical configuration of the computational domain of a constant pressure supersonic ejector was done according to the experimental setup of Bartosiewicz et al. (2005) and Desevaux (2001), shown in "Fig. 3".

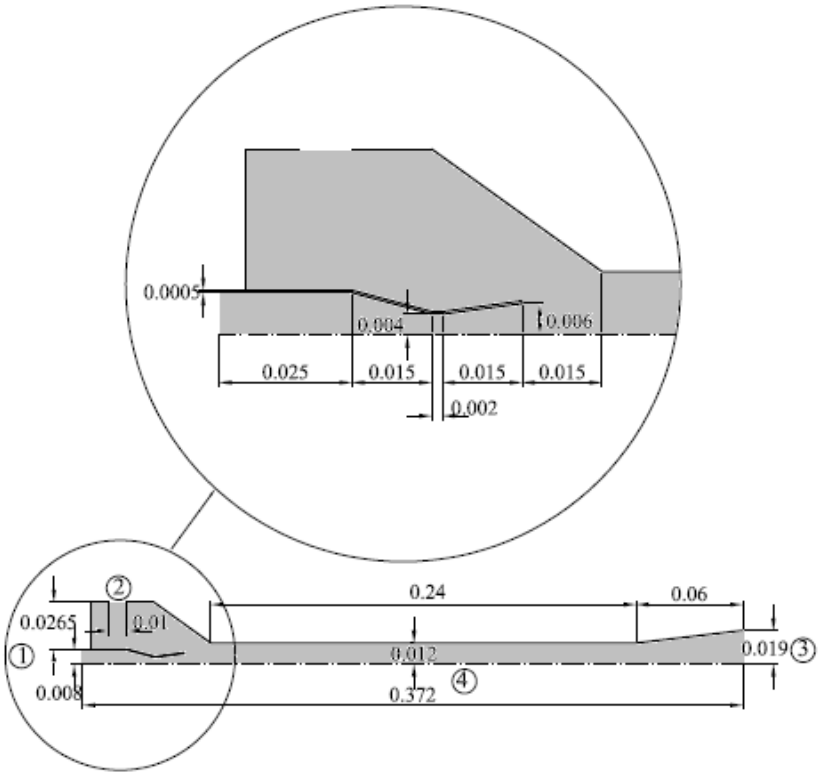

Figure 3. Geometric parameters of the constant pressure supersonic ejector (dimensions in m).

At surface 1, Fig. 3, or primary fluid inlet, the total pressure and total temperature, and normal flow direction to input surface are prescribed. At surface 2, secondary fluid inlet, total temperature and mass flow rate are prescribed, and in the surface 3, or exit, the static pressure is imposed. At all inlet boundaries, 5% for turbulent intensity and 5 for turbulent viscosity ratio are specified, while, axisymmetrical boundary condition is prescribed at surface 4. All the walls are considered to be adiabatic with no slip and enhanced wall law are used as turbulence model boundary conditions. Numerical values for inlet and outlet boundary conditions are shown in Tab. (2).

Table 2. Surfaces, boundary condition type, boundary conditions and values.

Surfaces	Boundary condition type	Prescribed Boundary Values	
1	Pressure inlet	T_{Total} = 300 K	P_{Total} = 4; 5 atm
2	Mass flow rate	T_{Total} = 300 K	$\dot{m}$ = 0.020; 0.024; 0.028; 0.030; 0.032; 0.036; 0.040; 0.044; 0.048 kg/s
3	Pressure outlet	T_{Total} = 300 K	P_{static} = 1 atm

4. COMPUTATIONAL STRATEGY

The numerical simulations have been performed using the commercial CFD package FLUENT (12.1), Fluent (2008), based on finite volume methods (FVM). The compressible, turbulent, axisymmetric, steady state flow was calculated using a pseudo-transient technique with a density based approach**.** The turbulence models utilized were realizable – k–ε or sst –k – ω. The transient formulation was first order implicit. The numerical approximation utilized was first order for the advective terms and pressure. During algebraic equations system iterative solution, CFL is set to 1.

5. RESULTS

On the simulations, the domain shown in Fig. 3 was used, which is based on the geometric parameters of Bartosiewicz et al. (2005) and Desevaux (2001).

Firstly, it has been done a validation comparing with Bartosiewicz et al. (2005) results to analyze the performance of realizable – k– ε or sst – k– ω turbulence models. For these tests, there is no secondary flow, the inlet pressure is P_{Total} = 5 atm, the graphic was plotted from the primary nozzle outlet and P_r = 5 atm taken as reference.

Figure 4 illustrates results for the axial pressure obtained with realizable – k– ε or sst – k– ω turbulence models and also the experimental ones of Bartosiewicz et al. (2005). Performance of sst – k– ω turbulence model is better than realizable – k– ε for ejector modeling. Based in this comparison, sst – k– ω turbulence model was used to obtain the following results.

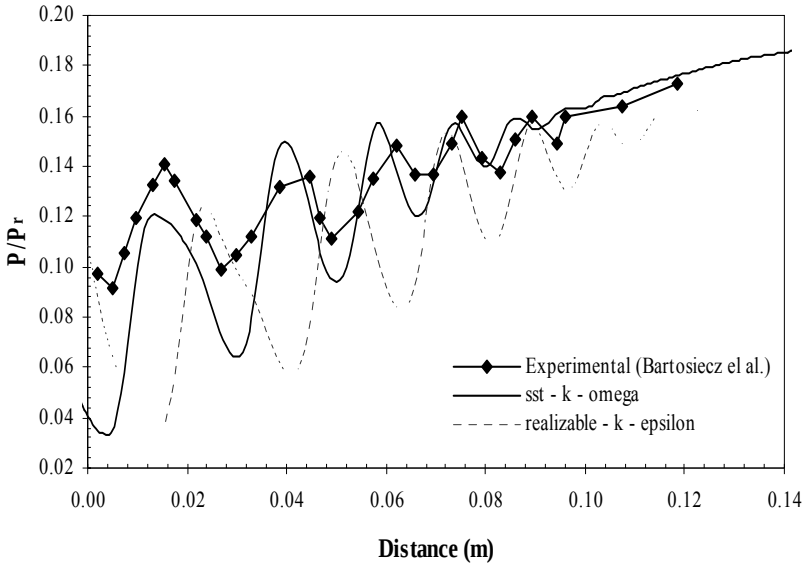

Figure 4. Comparison between the sst – k– ω and the realizable – k– ε model for no secondary flow.

In Fig. 5, a comparison with Bartosiewicz et al. (2005) results. In present work numerical results were obtained with convective terms first order discretization and sst – k– ω turbulence model for an ejector with induced secondary flow ($\dot{m}$ = 0.028 kg/s). In this case, the primary flow inlet pressure was P_{Total} = 4atm. There was a shift in the first

pressure oscillation, however, this phase difference was reduced for posterior oscillations. Numerical results present more oscillations than experimental ones.

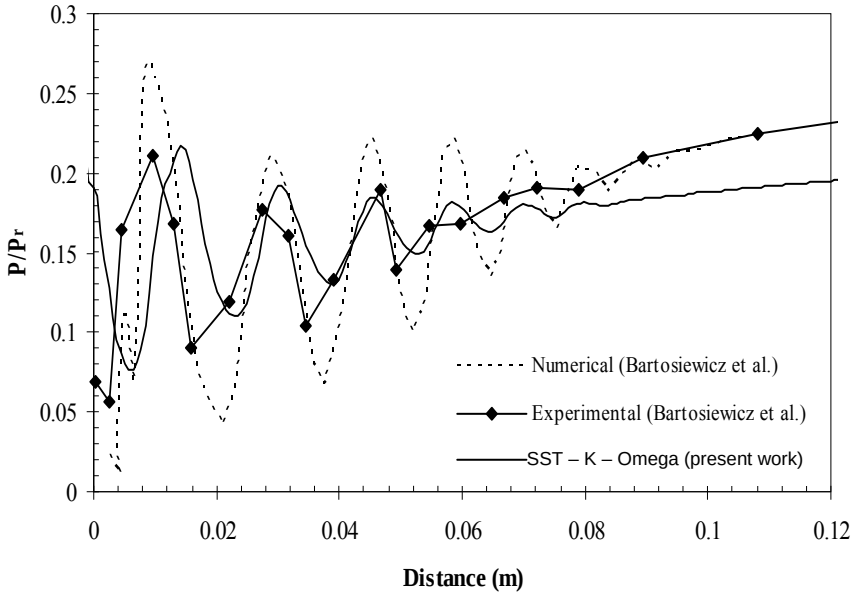

Figure 5. Axial pressure sst – k– ω model with secondary flow.

In order to find out the optimum length of the constant pressure mixing chamber, 7 ejectors, in a total of 28 cases, were studied by varying of length of mixing chamber and mass flow on secondary inlet. The mass flow on secondary inlet ranges from 0.02 to 0.032 kg/s and the pressure inlet remains at 4 atm.

Figure 5 shows variation of the length of constant pressure mixing chamber with the pressure difference between outlet and secondary inlet. The results indicate that the parameter length of mixing chamber have critical importance to the ejector performance and should be carefully designed inside the optimum range. In these testes, for the ejector modeling, the optimum length was found according to Eq. (10), being that the lower mass flow in the secondary inlet greater the pressure difference (P_3-P_2) and thus produces better performance.

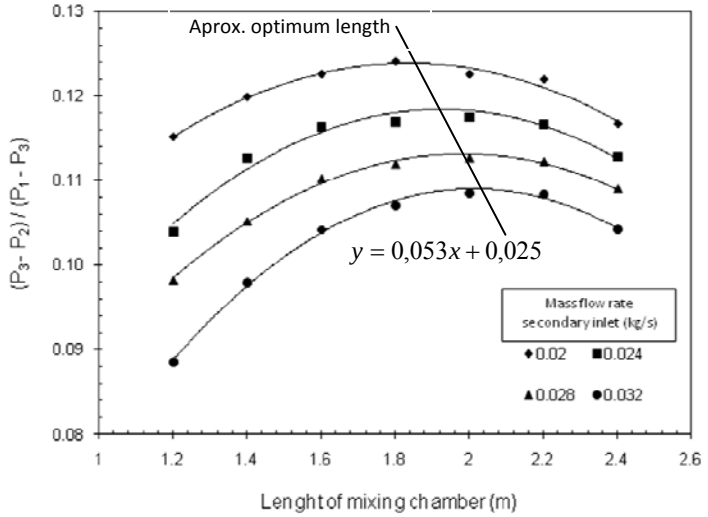

Figure 5. Analysis of constant pressure mixing chamber length.

Note that for each curve there is a maximum point, then, one can conclude that there is an optimum length for the mixing chamber of constant pressure, the behavior observed for each discharge variation. By this equation is possible to obtain the optimum length of the mixing chamber for a given flow in the secondary input to the model of the ejector, where *x* represents the secondary flow and *y* the length.

$$y = 0{,}053x + 0{,}025 \tag{10}$$

6. CONCLUSION

In this work was performed a numerical simulation to analyze the performance of gas supersonic ejector, varying the constant pressure mixing chamber length and mass flow at secondary inlet. Two turbulence models (realizable k- ε and sst-k-ω turbulence models) were tested. The better agreement with experimental results of Bartosiewicz (2005) was obtained using sst-k-ω turbulence model. There was a greater shift differences in the first pressure oscillation that is reduced for posterior cycles.

In the tested, for the ejector modeling, the optimum length of constant pressure mixing chamber is found in the according to Eq. (10). This equation provides the ideal length of the mixing chamber for a given flow in the secondary entrance, where *x* represents the secondary flow and *y* the length, since this parameter is influenced by secondary flow. Being that the lower mass flow in the secondary inlet greater the pressure difference (P_3-P_2) and thus better performance.

7. ACKNOWLEDGEMENTS

The authors would like to acknowledge the CAPES by the financial support and the GSET (Group of Simulation of Flow and Heat Transfer) by the computational support.

8. REFERENCES

Bartosiewicz, Y., Aidoun, Z., Desevaux, P. and Mercadier, Y., 2005, "Numerical and experimental investigations on supersonic ejectors" , Int. J. of Heat and Fluid Flow, Vol. 26, pp. 56-70.

Bartosiewicz, Y., Aidoun, Z. and Mercadier, Y., 2006, "Numerical assessment of ejector operation for refrigeration applications based on CFD", Applied Thermal Engineering, Vol. 26, pp. 604-612.

Chunnanond, K. and Aphornratana, S., 2004a, "Ejectors: applications in refrigeration technology", Renewable and Sustainable Energy Reviews, Vol. 8, pp. 129-155.

Desevaux, P., 2001, "A method for visualizing the mixing zone between two co-axial flows in an ejector", Optics and Lasers in Engineering, Vol. 35, pp. 317-323.

FLUENT INC. User's guide, versão 12.0, 2008. Disponível em <www.fluent.com>. Acesso em 25 de maio. 2010.

Keenan, J.H., Neumann, E.P. and Lustwerk, F., 1950, "An investigation of ejector design by analysis and experiment", ASME J. Appl. Mech. Trans., Vol.72, pp.299–309.

Rusly, E., Aye, L., Charters, W.W.S., Ooi, A. and Pianthong, K., 2002, "Ejector CFD modeling with real gas model", Mechanical Engineering Network of Thailand the 16th Conference, pp.150–5.

Sriveerakul, T., Aphornratana, S. and Chunnanond, K., 2007a, "Performance prediction of steam ajector using computational fluid dynamics: Part 1. Validation of the CFD results", Int. J. of Thermal Sciences, Vol. 46, pp. 812-822.

Sriveerakul, T., Aphornratana, S. and Chunnanond, K., 2007b, "Performance prediction of steam ajector using computational fluid dynamics: Part 2. Flow structure of a steam ejector influenced by operating pressures and geometries", Int. J. of Thermal Sciences, Vol. 46, pp. 823-833.

Yinhai, Z., Wenjian, C., Changyun, W. and Yanzhong, L., 2009, " Numerical investigation of geometry parameters for design of high performance ejectors", Applied Thermal Engineering, Vol. 29, pp. 898-905.

9. RESPONSIBILITY NOTICE

The author(s) is (are) the only responsible for the printed material included in this paper.